15th International Heat Pipe Conference (15th IHPC), Clemson, USA, April 25-30, 2010.

An Inverse Methodology to Estimate the Heat Transfer Coefficient in the Evaporator Section of a CO_2 Single Loop Pulsating Heat Pipe

Franco Andrey Silvério de Souza
Refrigeration and Air Conditioning Department
Federal Institute of Technology (IFSC)
Praia Comprida, São José/SC, 88103-310, Brazil
Phone/Fax: +55 48 3721-9379
franco@lepten.ufsc.br

Sergio Colle, Júlio César Passos
Mechanical Engineering Department
Federal University of Santa Catarina (UFSC)
Trindade, Florianópolis/SC, 88040-900, Brazil
Phone/Fax: +55 48 3721-9379
colle@emc.ufsc.br, jpassos@emc.ufsc.br

ABSTRACT

This paper presents an analytical method based on a parameter estimation technique to estimate the convective heat transfer coefficient inside a single loop pulsating heat pipe (SLPHP), using carbon dioxide (CO_2) as the working fluid. The method leads to an ill-posed heat transfer problem whose solutions may become unstable, due to measurement errors inherent in the experimental data. For this reason, an approximate analytical expression is initially obtained for the temperature profile along the tube wall thickness, departing from the solution of the diffusion energy equation describing the heat transfer in the evaporator section. The expression obtained, together with the experimental parameters, forms the basis of the proposed method. The convective heat transfer coefficient is obtained through minimization of an ordinary least-squares objective function. The stabilization technique is the sequential linear function specification as reported in (Beck et al., 1985). The minimization is carried out with the conjugate gradient method. The above-mentioned method and the effectiveness of the minimization procedure are described in detail in Özisik and Orlande (2000).

KEYWORDS: Single loop pulsating heat pipes, carbon dioxide, heat transfer coefficient, inverse heat transfer, conjugate gradient method.

1. INTRODUCTION

Theoretical analysis with emphasis on the mathematical modeling of pulsating heat pipes has focused mainly on presenting a series of methodological and phenomenological simplifications, particularly due to the complex thermo-hydrodynamic operational characteristics of these devices. In this regard, Khandekar et al. (2003) elaborated a semi-empiric model to determine the maximum heat transfer achievable for closed loop pulsating heat pipes (CLPHPs), based on the concept of non-dimensional groups. Dobson and Graf (2003) proposed a definition for an average heat transfer coefficient for a CLPHP,

globally modeled and based on the concept of thermal resistance. A multi-linear regression analysis was used in order to obtain a correlation for the heat transfer coefficient.

Parameter estimation in heat transfer has been widely used over the past four decades, due to its effectiveness in determining the temperature, heat flux, heat transfer coefficient and thermal conductivity under different circumstances. The method has been successful in accounting for inhomogeneous materials, considering arbitrary geometries and non-linear functional dependence (Özisik and Orlande, 2000). The wall thickness in parameter estimation of heat transfer in the mini and micro-scale is one of the parameters to be considered, because thermal gradients may reduce the accuracy of the numerical techniques and, in this case, the wall temperature and the heat flux are considered to be the impute functions provided by experiments (Beck et al., 1985).

In the particular case of pulsating heat pipes, the wall thickness is comparable with the pipe diameter. The wall thickness parameter becomes more important for pipes made of steel, for which the thermal gradients are larger. In order to reduce thermal gradients in the evaporator wall, a pipe made of copper is chosen. The impute parameters considered are the outer tube wall and the heat flux impute on the outer surface. The heat transfer coefficient is defined in terms of the difference between the inner tube wall temperature (to be determined by the inverse method) and the experimentally measured fluid bulk temperature. This temperature is calculated by a saturation pressure correlation.

2. MATHEMATICAL MODEL

A cross section of the evaporator tube of a SLPHP, submitted to a given heat flux $q_e^{"}(t)$ at r_e and convection at r_i, with the heat coefficient $h_i(t)$, was considered as illustrated in Figure 1. In the present analysis only radial transient heat conduction in the tube wall is assumed. Internal heat generation in the wall is absent and the thermal conductivity of the wall material is independent of the temperature. With the above assumptions, the diffusion energy equation is reduced to the following:

$$\frac{1}{r}\frac{\partial}{\partial r}\left[r\frac{\partial T(r,t)}{\partial r}\right]=\frac{1}{\alpha}\frac{\partial T(r,t)}{\partial t},\ \text{at}\ r_i<\mathrm{r}<r_e\ \text{and}\ t>0 \qquad (1)$$

The following boundary conditions hold:

$$-\lambda\frac{\partial T(r,t)}{\partial r}=-h_i(t)\left[T(r_i,t)-T_{bulk}(t)\right],\ \text{at}\ r=r_i\ \text{and}\ \mathrm{t}>0 \qquad (2)$$

$$\lambda\frac{\partial T(r,t)}{\partial r}=q_e^{"}(t),\ \text{ at }\ r=r_e\ \text{ and }\ t>0 \qquad (3)$$

The initial condition is given by:

$$T(r,t)=F(r)=T_0,\ \text{at}\ \ r_i<\mathrm{r}<\mathrm{r_e}\ \ \text{and}\ \ t=0 \qquad (4)$$

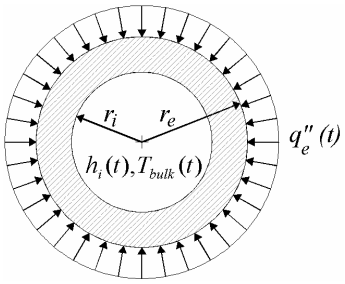

Figure 1. Geometric and thermal parameters for the evaporator tube cross section of the SLPHP.

Equations (1) to (4) pose a non-homogeneous (at r_i and r_e) boundary value problem (BVP) where the coefficient $h_i(t)$ is unknown. The general solution of this BVP can be obtained in a straightforward fashion using the Green function method described in (Stakgold, 1968). The Green function is a solution of the homogeneous BVP given by the following equations:

$$\frac{1}{r}\frac{\partial}{\partial r}\left[r\frac{\partial G(r,t\mid r',t')}{\partial r}\right]=\frac{1}{\alpha}\frac{\partial G(r,t\mid r',t')}{\partial t},\ \text{at}\ \ r_i<\mathrm{r}<r_e\ \text{and}\ \ t>t' \qquad (5)$$

$$\lambda\frac{\partial G(r,t\mid r',t')}{\partial r}=0,\ \ \text{for}\ \ r=r_i\ \ \text{and}\ \ \mathrm{t}>t' \qquad (6)$$

$$\lambda\frac{\partial G(r,t\mid r',t')}{\partial r}=0,\ \ \text{for}\ \ r=r_e\ \ \text{and}\ \ \mathrm{t}>\mathrm{t}' \qquad (7)$$

The Green functions vanish for $t = t'$. The temperature distribution in the tube wall has been shown to be expressed by the integral equation form given by Equation (5). The analytical details proposed for several different boundary conditions can be found in Özişik, (1993).

$$
\begin{aligned}
&T(r,t) = \frac{2}{r_e^2 - r_i^2} T_0 \int_{r_i}^{r_e} r' dr' + \\
&\sum_{m=1}^{\infty} \frac{R_0(\beta_m, r)}{N(\beta_m)} e^{-\alpha \beta_m^2 \, t} \int_{r_i}^{r_e} r' R_0(r') F(r') \, dr' - \\
&\frac{\alpha r_i}{\lambda} \frac{2}{r_e^2 - r_i^2} \int_0^t h_i(t') [T(r_i, t') - T_{bulk}(t')] \, dt' - \\
&\frac{\alpha r_i}{\lambda} \sum_{m=1}^{\infty} \frac{R_0(\beta_m, r) \, R_0(\beta_m, r_i)}{N(\beta_m)} \int_0^t h_i(t') [T(r_i, t') - T_{bulk}(t')] e^{-\alpha \beta_m^2 \, (t - t')} dt' \\
&\frac{\alpha r_e}{\lambda} \frac{2}{r_e^2 - r_i^2} \int_0^t q_e''(t) \, dt' + \\
&\frac{\alpha r_e}{\lambda} \sum_{m=1}^{\infty} \frac{R_0(\beta_m, r) \, R_0(\beta_m, r_e)}{N(\beta_m)} \int_0^t q_e''(t) \, e^{-\alpha \beta_m^2 \, (t - t')} dt'
\end{aligned}
\tag{5}
$$

where $R_0(\beta_m, r)$ stands for the eigenfunction, and $N(\beta_m)$ and β_m are the integral norm and eigenvalue, respectively.

The temperature on the tube wall, expressed by Equation (5), is determined through a knowledge of $h_i(t')$ and $T(r_i, t')$. In order to determine these unknown functions they are expressed in terms of linear tent functions, discretized in time with unknown coefficients a_j and b_j, respectively. Both, $q_e''(t)$, $T_{bulk}(t')$ and $T(r_e, t)$, the latter expressed by Equation (7), are also expressed as tent functions, in terms of the coefficients q_j, c_j and d_j, which are experimentally determined. Figure 2 shows the tent function representation for the heat transfer coefficient.

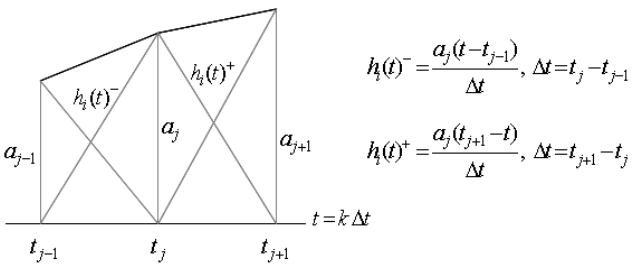

Figure 2. Illustration of the composition of the tent functions for the heat transfer coefficient.

Equation (5) can thus be reduced to the following algebraic equations:

$$T(r_i, t) = b_k = G_k^i - \sum_{j=1}^{k} B_{kj}^{is-+} \, a_j (b_j - c_j) + \sum_{j=1}^{k} D_{kj}^{is-+} \, q_j \tag{6}$$

$$T(r_e, t) = d_k = G_k^e - \sum_{j=1}^{k} B_{kj}^{es-+} \, a_j \, (b_j - c_j) + \sum_{j=1}^{k} D_{kj}^{es-+} \, q_j \tag{7}$$

The coefficients B, G and D, which appear in Equations (6) and (7), are presented in the Appendix. The unknowns of this equations are therefore a_j, b_j. In order to set a third equation for the ill-posed problem given by Equations (6) and (7), the following objective function to be minimized is proposed:

$$S = \sum_{k=1}^{p} (Y_k - d_k)^2 \tag{8}$$

This equation expresses the sum of squares of the difference between the measured outer tube temperature and d_k, which is expressed by Equation (7). The set of equations obtained by minimizing S is given as follows.

$$\frac{\partial S}{\partial a_j} = 2 \sum_{k=1}^{p} \left(-\frac{\partial d_k}{\partial a_j} \right) \left(Y_k - d_k \right) = 0; \; j = 1,2,...N_a \tag{9}$$

where N_a is the number of discretizations. The function specification representation for the heat transfer coefficient is illustrated in Figure 3.

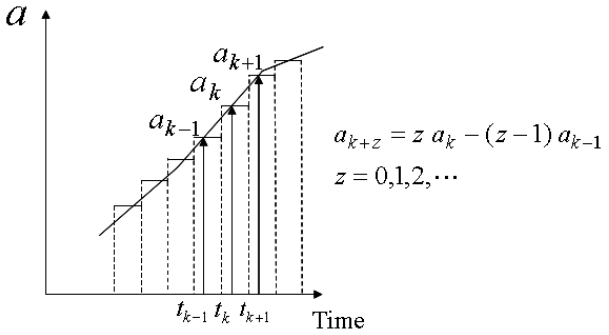

Figure 3. Illustration of the linear heat transfer coefficient functional form.

The nonlinear preconditioned conjugate gradient method of Polak-Ribière and Newton-Raphson (Shewchuck, 1994) is applied to simultaneously determine a_k and d_k.

3. EXPERIMENTAL SETUP

An experimental setup was designed in order to obtain the experimental parameters necessary for the estimation of the convective heat transfer coefficient inside the pulsating heat pipe evaporator. For this purpose, a single loop pulsating heat pipe (SLPHP) made of copper is designed according to the specifications given in Table 1. The condenser was inserted in the interior of a manifold, through which the cooling fluid ethanol is supplied by a thermostatic bath. The evaporator is heated by an electrical resistance coil controlled by a DC power supply. In order to achieve good insulation, the SLPHP assembly was fully enclosed inside a vacuum chamber where a low pressure ($<10^{-3}$ mbar) was maintained by continuously running a vacuum pump. A thermal radiation shield is placed around the evaporator to prevent radiation losses. Type-T thermocouples are installed on the tube outer surface, in the evaporator, in the condenser, and in the adiabatic section. A subminiature pressure transducer is installed close to the evaporator. The working fluid bulk temperature is determined from a saturation pressure correlation. The filling ratio, the angle inclination from the horizontal, and the cooling bath temperature considered are 60%, 90° and -30°C, respectively, for all tests. The data acquisition is carried out by a National data logger model SCXI-1000. The measuring system is calibrated in terms of the temperature and pressure against laboratory recognized standards available at the Laboratory of Refrigeration and Air-Condition of the Department of Mechanical Engineering of UFSC. The experiment is controlled using the software program LabView, with a measuring frequency of 20 Hz. The maximum variation of internal pressure observed in each acquisition time interval was lower than 0.1 bar. The uncertainty of the measurement devices used in the experiments are summarized in Table 2.

Table 1. SLPHP design characteristics.

Evaporator length	33.16 mm
Condenser length	240 mm
Adiabatic section length	307 mm
Total tube length	580 mm
Tube inner diameter	1.27 mm
Tube external diameter	2.4 mm
Tube roughness	0.63 μm

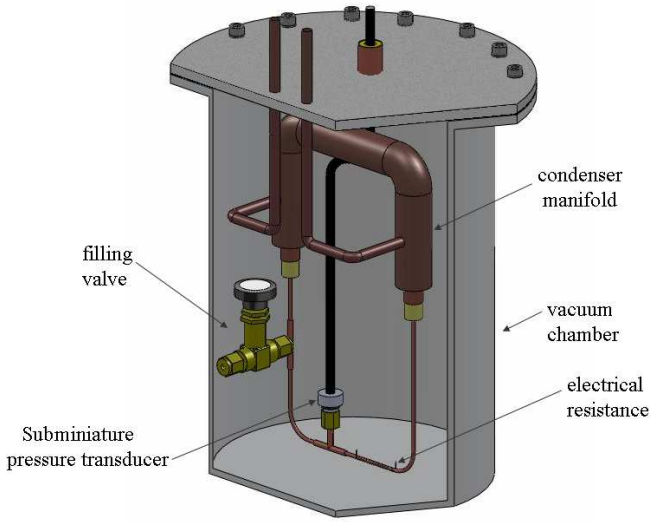

Figure 5. Schematic drawing of the SLPHP and vacuum chamber.

Table 2. Uncertainty of the measurement devices used in the experimental setup.

Device	Range	Uncertainty
Termocouple	-40 to 40 °C	±0.1 °C
Pressure transducer	0 to 100 bar	±0.05 bar

4. RESULTS AND DISCUSSION

4.1. Experimental Parameters

As previously described, the estimation of the film convective heat transfer coefficient assumes, besides the mathematical model, the experimental acquisition of the heat flux, of the tube external wall temperature, and the working fluid bulk temperature in the evaporator section. The first two parameters are directly obtained from the experimental apparatus of Figure 5 and the bulk temperature is obtained using Equation (10).

$$T_{sat}[^oC] = -69.949 + 3.668P_{sat}[bar] - 0.0735P_{sat}^2[bar] + 0.000896P_{sat}^3[bar] + 0.00000439P_{sat}^4[bar] \quad (10)$$

Figures 6 to 9 show experimental results obtained for seven distinct heat fluxes. Each test began only when the average temperatures on the evaporator and condenser outer surfaces reached their lower stabilization levels. Figure 6 shows the transient variation of absolute pressure inside the evaporator of the SLPHP. Figures 7 to 9 show the transient variations of the bulk temperature (obtained from Equation 10), average evaporator outer wall temperature and average condenser outer wall temperature. It can be seen from these figures that the bulk temperature always lies between the condenser and evaporator temperatures, as expected.

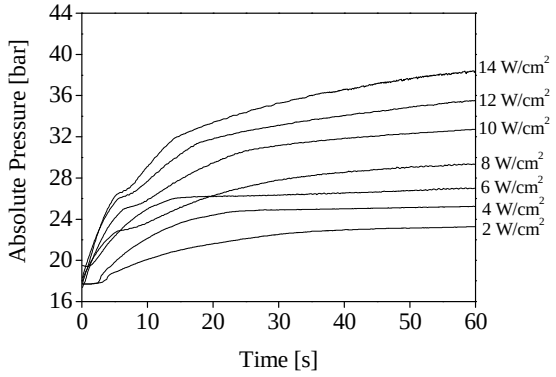

Figure 6. Transient variation of the pressure inside the evaporator.

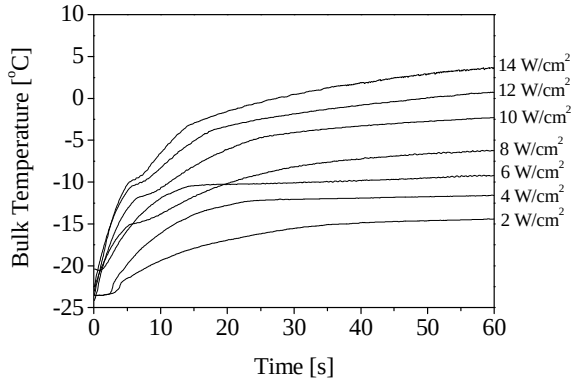

Figure 7. Transient variation of the working fluid bulk temperature.

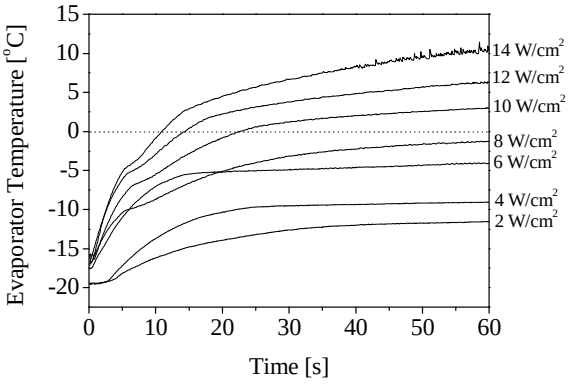

Figure 8. Transient variation of the average evaporator outer wall temperature.

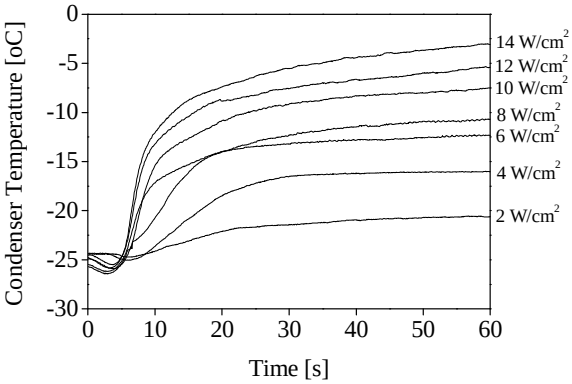

Figure 9. Transient variation of the average condenser outer wall temperature.

4.2 Convective Heat Transfer Coefficient

The experimental parameters, together with the proposed mathematical model, may now be used in order to estimate the convective heat transfer coefficient. For this purpose, two possibilities are considered: Firstly, the heat transfer coefficient is considered constant and, secondly, time dependence is admitted, represented by the following equation:

$$h_i(t) = u(q_e'')\,\tau^{0.1}, \text{ where } \tau = \frac{\alpha}{r_i^2}t \quad (11)$$

Table 2 shows the calculated values for the constant heat transfer coefficient using the experimental parameters of Figures 7, 8 and 9. Figure 10 shows a comparison between the experimental averaged evaporator outer wall temperature and the calculated temperature using Equation (7) and the coefficients of Table 2. According to Figure 10 the predicted evaporator outer wall temperature is in good agreement with the measured temperature.

Table 2. Calculated constant heat transfer coefficient.

Heat flux [W/cm²]	Heat transfer coefficient [W/m²K]
2	18692.6
4	25008.0
6	36153.3
8	46778.5
10	56103.7
12	64955.4
14	68211.1

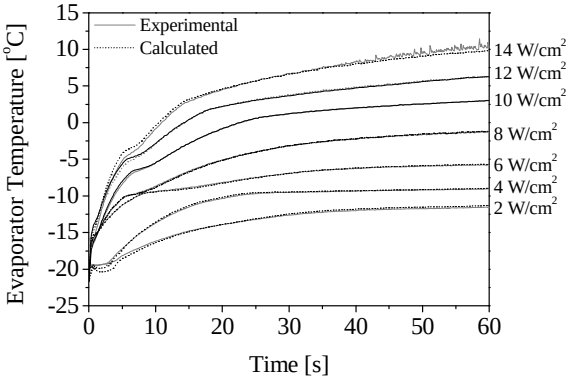

Figure 10. Comparison between the experimental average evaporator outer wall temperature and the predicted temperature obtained from Equation (7), for the constant heat transfer coefficient given in Table 2.

Figure 11 shows the time-dependent heat transfer coefficient modeled according to the correlation given by Equation (11). The respective numerical values of the factor $u(q_e'')$, determined by parameter estimation, is given in Table 3.

Table 3. Calculated $u(q_e'')$ for time-dependent heat transfer coefficient.

Heat flux [W/cm²]	$u(q_e'')$ [W/m²K]
2	5579.3
4	10341.7
6	14958.3
8	19358.2
10	23212.4
12	26694.1
14	27777.4

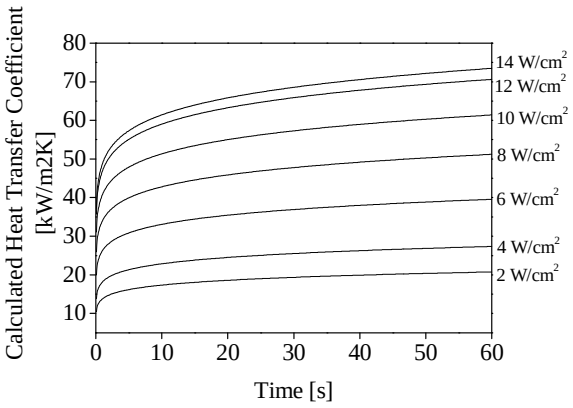

Figure 11. Calculated time-dependent heat transfer coefficient.

Figure 12 shows a comparison between the experimental average evaporator outer wall temperature and the calculated temperature using Equations (7) and (11), for the coefficients given in Table 3. In this case, the predicted results are not in as good agreement as those for the case assuming a constant heat transfer coefficient. However, these results are acceptable considering the uncertainty currently obtained in experiments to determine the convective heat transfer coefficient. Correlations other than that given by Equation (11) can be assumed in order to describe the best correlation for the heat transfer coefficient. The question of whether there is a better time-dependent correlation for the heat transfer coefficient for the evaporator of the SLPHP remains unresolved.

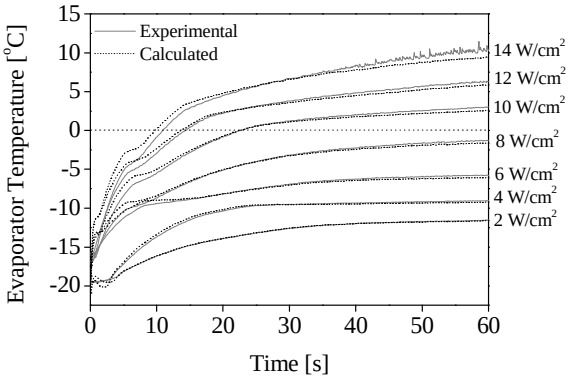

Figure 12. Comparison between the experimental average evaporator outer wall temperature and the temperature calculated using Equations (7) and (11) and the coefficients of Table 3.

4.3 Results Comparison

Gorenflo and Kotthoff (2005) provided an extensive review on the pool boiling heat transfer of carbon dioxide. Among the studies reviewed, Kotthoff et al. (2004) reports experimental results obtained under similar conditions to those of this study.

The pool boiling heat transfer was obtained outside a horizontal copper tube with 8 mm of inner diameter and 0.62 of roughness, for a wide range of heat fluxes (0.002 up to 10 Wcm^{-2}), and saturation pressures (5.18 up to 46.12 bar) and temperatures (-56.56 up to 10.91 °C). These saturation pressure and temperature ranges cover the conditions under which Figures 6 and 7 were obtained (17.36-38.44 bar and -24.15 to 3.72 °C, respectively). Table 4 shows a comparison between the calculated heat transfer coefficients shown in Table 2 and the heat transfer coefficients reported in the previously cited studies.

Apart from phenomenological differences, the heat transfer coefficients obtained in this study are consistent with those obtained experimentally by Kotthoff et al. (2004).

5. CONCLUSIONS

A method is proposed herein to estimate the convective heat transfer coefficient for the boiling heat transfer in the evaporator of a CO_2 single loop pulsating heat pipe. The experimental setup to measure the parameters required to evaluate the heat transfer coefficient using the proposed parameter estimation technique is also described.

The predicted outer wall evaporator temperature is shown to be in good agreement with the experimental results, by assuming a constant heat transfer coefficient over time. The time-dependent heat transfer coefficient assumed here led to an agreement of the results which was not as good as that of the constant heat transfer coefficient.

It can be concluded that the method proposed herein can be applied to other situations where more complex factors are considered, for instance, the heat transfer in boiling heat transfer on enhanced surfaces or surfaces with large capillary forces. However, at the present time, general methods to obtain analytically the temperature distribution over regions of arbitrary shapes are currently unavailable (Cotta, 1998).

Table 4. Comparison between the calculated heat transfer coefficients and those of Kotthoff et al. (2004).

Mean saturation temperature of CO_2 (mean bulk temperature) [°C]	Heat flux [W/cm²]	Heat transfer coefficient		Error [%]
		Present study [W/m²]	Kotthoff et al. (2004)* [W/m²]	
-13.64	2	18692.6	≈ 17100	9.31
-14.05	4	25008.0	≈ 29300	14.65
-10.99	6	36153.3	≈ 41900	13.72
-9.71	8	46778.6	≈ 56900	17.79
-6.15	10	56103.7	≈ 68500	18.10

* interpolated values from Figure 1 of the original paper

NOMENCLATURE

a	: heat transfer coefficient, W/m^2
b	: tube inner wall temperature coefficient, °C
d	: tube diameter, m
	: tube outer wall temperature coefficient, °C
F_0	: arbitrary function
h	: convective heat transfer coefficient, W/m^2
n	: number of discretized times
N	: norm, /m^2
P	: pressure, bar
q	: heat flux coefficient, W/m^2
q''	: heat flux, W/m^2
r	: radius, m
R_0	: eigenfunction
T	: temperature, °C
t	: time, s

Greek Symbols

α	: thermal diffusivity, m^2/s
β	: eigenvalue
λ	: thermal conductivity, W/mK

Subscripts

bulk	: related to carbon dioxide flow
i	: inner
e	: outer
sat	: saturation

Abbreviations

SLPHP	: single loop pulsating heat pipe
CLPHP	: closed loop pulsating heat pipe
BVP	: boundary value problem

ACKNOWLEDGEMENT

The authors are grateful to the National Research Council of Brazil (CNPq) for funding this study under the supervision of Prof. S. Colle, and also to IFSC for logistical help.

REFERENCES

1. COTTA, R. M., *The Integral Transform Method in Thermal and Fluid Science and Engineering*, Begell House, New York, 1998.

2. BECK J. V., BlackWell B. and St. Clair Jr. C. R., *Inverse Heat Conduction: Ill-posed Problems*, John Wiley & Sons, New York, 1985.

3. DOBSON R. T. and GRAF G., Thermal Characterization of an Ammonia-charged Pulsating Heat Pipe, Proc. 7th Int. Heat Pipe Symp., Stellenbosch, South Africa, 2003.

4. GORENFLO D. and KOTTHOFF S., Review on Pool Boiling Heat Transfer of Carbon Dioxide, *International Journal of Refrigeration*, Vol. 28, pp. 1169-1185, 2005.

5. KHANDEKAR S.; CHAROENSAWAN P.; GROLL M. and TERDTOON P., Closed Loop Pulsating Heat Pipes – Part B: Visualization and Semi-Empirical Modeling, *Applied Thermal Engg*., Vol. 23/16, pp. 2021-2033, 2003.

6. KOTTHOFF S, CHANDRA U. and GORENFLO D., New Measurements of Pool Boiling Heat Transfer for Carbon Dioxide in a Wide Temperature Range, *Proceedings of Sixth IIR – Gustav Lorentzen Conference*, Glasgow, England, 2004.

7. ÖZIŞIK M. N. and ORLANDE H. R. B., *Inverse Heat Transfer: Fundamental and Applications*, Taylor & Francis, New York, 2000.

8. ÖZIŞIK M. N. *Heat Conduction*, John Wiley & Sons, New York, 1993.

9. SHEWCHUCK J. R., An Introduction to the Conjugate Gradient Method Without the Agonizing Pain, School of Computer Science, Carnegie Melon University, Pittsburgh, USA, 1994.

10. STAKGOLD, I., *Boundary Value Problems of Mathematical Physics*, Vol. II, Macmilan Series in Advanced Mathematics and Theoretical Physics, New York, 1968.

APPENDIX

$$B_{kj}^{is-+} = \frac{\alpha r_i}{\lambda}(B_{kj}^{0i-} + B_{kj}^{0i+} + B_{kj}^{i-} + B_{kj}^{i+}) \tag{12}$$

$$B_{kj}^{es-+} = \frac{\alpha r_e}{\lambda}(B_{kj}^{0e-} + B_{kj}^{0e+} + B_{kj}^{e-} + B_{kj}^{e+}) \tag{13}$$

$$B_{kj}^{i-} = \sum_{m=1}^{\infty} \frac{{R_0}^2(\beta_m, r_i)}{N(\beta_m)} A_{mkj}^{-} \tag{14}$$

$$B_{kj}^{i+} = \sum_{m=1}^{\infty} \frac{{R_0}^2(\beta_m, r_i)}{N(\beta_m)} A_{mkj}^{+} \tag{15}$$

$$B_{kj}^{e-} = \sum_{m=1}^{\infty} \frac{R_0(\beta_m, r_i) R_0(\beta_m, r_e)}{N(\beta_m)} A_{mkj}^{-} \tag{16}$$

$$B_{kj}^{e+} = \sum_{m=1}^{\infty} \frac{R_0(\beta_m, r_i) R_0(\beta_m, r_e)}{N(\beta_m)} A_{mkj}^{+} \tag{17}$$

$$D_{kj}^{i-} = \sum_{m=1}^{\infty} \frac{R_0(\beta_m, r_i) R_0(\beta_m, r_e)}{N(\beta_m)} C_{mkj}^{-} \tag{18}$$

$$D_{kj}^{i+} = \sum_{m=1}^{\infty} \frac{R_0(\beta_m, r_i) R_0(\beta_m, r_e)}{N(\beta_m)} C_{mkj}^{+} \tag{19}$$

$$D_{kj}^{e-} = \sum_{m=1}^{\infty} \frac{{R_0}^2(\beta_m, r_e)}{N(\beta_m)} C_{mkj}^{-} \tag{20}$$

$$D_{kj}^{e+} = \sum_{m=1}^{\infty} \frac{{R_0}^2(\beta_m, r_i)}{N(\beta_m)} C_{mkj}^{+} \tag{21}$$

$$B_{kj}^{0i-} = B_{kj}^{0e} = \frac{2}{r_e^2 - r_i^2} B_{mkj}^{0-} \tag{22}$$

$$B_{kj}^{0i+} = B_{kj}^{0e+} = \frac{2}{r_e^2 - r_i^2} B_{mkj}^{0+} \tag{23}$$

$$D_{kj}^{0i-} = D_{kj}^{0e} = \frac{2}{r_e^2 - r_i^2} D_{mkj}^{0-} \tag{24}$$

$$D_{kj}^{0i+} = D_{kj}^{0e+} = \frac{2}{r_e^2 - r_i^2} D_{mkj}^{0+} \tag{25}$$

$$B_{kj}^{is-+} = \frac{\alpha r_i}{\lambda}(B_{kj}^{0i-} + B_{kj}^{0i+} + B_{kj}^{i-} + B_{kj}^{i+}) \tag{26}$$

$$B_{kj}^{es-+} = \frac{\alpha r_e}{\lambda}(B_{kj}^{0e-} + B_{kj}^{0e+} + B_{kj}^{e-} + B_{kj}^{e+}) \tag{27}$$

$$D_{kj}^{is-+} = \frac{\alpha r_e}{\lambda}(D_{kj}^{0i-} + D_{kj}^{0i+} + D_{kj}^{i-} + D_{kj}^{i+}) \tag{28}$$

$$D_{kj}^{es-+} = \frac{\alpha r_e}{\lambda}(D_{kj}^{0e-} + D_{kj}^{0e+} + D_{kj}^{e-} + D_{kj}^{e+}) \tag{29}$$

$$G_k^i = T_0 + \sum_{m=1}^{\infty} \frac{R_0(\beta_m, r_i)}{N(\beta_m)} e^{-\alpha\beta_m^2 t_k} T_0 \int_{r_i}^{r_e} r' R_0(\beta_m, r') dr \tag{30}$$

$$G_k^e = T_0 + \sum_{m=1}^{\infty} \frac{R_0(\beta_m, r_e)}{N(\beta_m)} e^{-\alpha\cdot\beta_m^2 t_k} T_0 \int_{r_i}^{r_e} r' R_0(\beta_m, r') dr \tag{31}$$

$$B_{mkj}^{0-} = B_{mkj}^{0+} = \frac{\Delta t}{3} \tag{32}$$

$$D_{mkj}^{0-} = D_{mkj}^{0+} = \frac{\Delta t}{2} \tag{33}$$

$$A_{mkj}^{-} = \frac{1}{\alpha\beta_m^2}\left\{e^{-\alpha\beta_m^2 (k-j)\Delta t} - \frac{2}{\alpha\beta_m^2 \Delta t}\left[e^{-\alpha\beta_m^2 (k-j)\Delta t} - \left(\frac{e^{-\alpha\beta_m^2\cdot(k-j)\Delta t} - e^{-\alpha\beta_m^2 (k-j+1)\Delta t}}{\alpha\beta_m^2 \Delta t}\right)\right]\right\}, \text{for } j \le k \tag{34}$$

$$A_{mkj}^{+} = -\frac{1}{\alpha\beta_m^2}\left\{e^{-\alpha\beta_m^2 (k-j)\Delta t} + \frac{2}{\alpha\beta_m^2 \Delta t}\left[e^{-\alpha\beta_m^2 (k-j)\Delta t} + \left(\frac{e^{-\alpha\beta_m^2 (k-j)\Delta t} - e^{-\alpha\beta_m^2 (k-j+1)\Delta t}}{\alpha\beta_m^2 \Delta t}\right)\right]\right\}, \text{for } j \le k-1 \tag{35}$$

$$C_{mkj}^{-} = \frac{1}{\alpha\beta_m^2}\left[e^{-\alpha\beta_m^2 (k-j)\Delta t} - \left(\frac{e^{-\alpha\beta_m^2 (k-j)\cdot\Delta t} - e^{-\alpha\beta_m^2 (k-j+1)\cdot\Delta t}}{\alpha\beta_m^2 \Delta t}\right)\right], \text{for } j \le k \tag{36}$$

$$C_{mkj}^{+} = -\frac{1}{\alpha\beta_m^2}\left[e^{-\alpha\beta_m^2 (k-j)\Delta t} + \left(\frac{e^{-\alpha\beta_m^2 (k-j)\Delta t} - e^{-\alpha\beta_m^2 (k-j+1)\Delta t}}{\alpha\beta_m^2 \Delta t}\right)\right], \text{for } j \le k-1 \tag{37}$$